

Hydrate Formation During Transport of Natural Gas Containing Water And Impurities

Bjørn Kvamme*, Marthe Austrheim, Anette Knarvik, Mojdeh Zarifi
University Of Bergen, Department Of Physics And Technology, 5007 Bergen, Norway

ABSTRACT: The upper limit of water content permitted in a natural gas stream during its pipeline transport without a risk of hydrate formation is a complex issue. We propose a novel thermodynamic scheme for investigation of different routes to hydrate formation, with ideal gas used as reference state for all components in all phases including hydrate phase. This makes comparison between different hydrate formation routes transparent and consistent in free energy changes and associated enthalpy change. From a thermodynamic point of view natural gas hydrate can form directly from water dissolved in natural gas but quite unlikely due to limitations in mass and. The typical industrial way to evaluate risk of hydrate formation involves calculation of water condensation from gas and subsequent evaluation of hydrate from condensed water and hydrate formers in the natural gas. Transport pipes are rusty even before they are mounted together to transport pipelines. This opens up for even other routes to hydrate formation which starts with water adsorbing to rust and then leads to hydrate formation with surrounding gas. Rust consist on several iron oxide forms but Hematite is one of the most stable form and is used as a model in this study, in which we focus on maximum limits of water content in various natural gas mixtures that can be tolerated in order to avoid water dropping out as liquid or adsorbed and subsequently forming hydrate. Calculations for representative gas mixtures forming structure I and II hydrates are discussed for ranges of conditions typical for North Sea. The typical trend is that the estimated tolerance for water content is in the order of 20 times higher if these numbers are based on water dew-point rather than water dropping out as adsorbed on Hematite. For pure methane the maximum limits of water to be tolerated decrease with increasing pressures from 50 to 250 bars at temperatures above zero Celsius and up to six Celsius. Pure ethane and pure propane show the opposite trend due to the high density non-polar phase at the high pressures. Typical natural gas mixtures is, however, dominated by the methane so for systems of 80 per cent methane or more the trend is similar to that of pure methane with some expected shifts in absolute values of water drop-out mole-fractions.

Keywords: gas hydrates, natural gas transport, rust, alternative formation routes

NOMENCLATURE

C Number of components in the Gibbs phase rule
 E_p Potential energy [kJ/mol]
F Number of degrees of freedom in the Gibbs phase rule
 F Free energy [kJ/mol]
 f Free energy density [kJ/(mol m³)]
 f_i Fugacity [Pa]
 $g(r)$ Radial distribution function (RDF)
 G Gibbs free energy [kJ/mol]
 Δg_{kj}^{inc} Gibbs free energy of inclusion of component k in cavity type j [kJ/mol]
 H Enthalpy [kJ/mol]
 h_{kj} Cavity partition function of component k in cavity type j
k Cavity type index
K Ratio of gas mole-fraction versus liquid mole-fraction for the same component (gas/liquid K-values)
 N_i Number of molecules
N Number of phases in the Gibbs phase rule
 P Pressure [Pa]
 P_0 Reference pressure [Pa]
r Distance [m]

* Corresponding author: Phone: +47 934 51 956 E-mail: bjorn.kvamme@uib.no

- R Molar gas constant [kJ/(K mol)]
 T Temperature [K]
 T_c Critical temperature [K]
 v_j No. of type j cavities per water molecule
 v_m Molar volume [m³/mol]
 \bar{V}_r Molar volume of r th component [m³/mol]
 \bar{V}^{clath} Volume of clathrate [m³]
 x Mole fraction
 y_w Mole fraction of water
 Y Residual chemical potential per Kelvin
 z Mole fraction
 α Liquid (water) phase fraction
 β Inverse of the gas constant times temperature
 μ Chemical potential [kJ/mol]
 $\mu_w^{0,H}$ Chemical potential for water in empty hydrate structure [kJ/mol]
 θ_{kj} Fractional occupancy of cavity k by component j
 γ Activity coefficient
 ϕ Order parameter
 ρ Molar density [kg/m³]

I. INTRODUCTION

Pipeline transport of large volumes of natural gas at low temperatures and high pressures is a continuous operation. In the North Sea alone there is about 7800 km of pipeline transporting in the order of 96 billion standard cubic meter of gas per year. Most of the transport lines lie on the seafloor and are exposed to temperatures 2 – 6°C. With pressures spanning the range from 200 atm to that at receiving terminals, large portion, if not all, of the pipeline transport will occur within hydrate formation conditions. Under these conditions, transported gas mixtures have shown a tendency to form ice like structures, known as clathrate hydrates (cf. ¹ and references therein). Hydrate nucleation and growth within a dense stream of natural gas with significant admixtures of impurities (limited to water in this work) is a complex process involving competing phase transition mechanisms and pathways, where both kinetics and thermodynamics play an important role. Schemes currently employed by the industry to evaluate hydrate risks assume that hydrate formation will be determined by dropout of water within the gas bulk and thus calculate the dew-point temperature of the given mixture. This approach completely ignores the fact that the presence of rust on the pipeline walls will provide water adsorption sites and thus add additional pathways for hydrate formation.

The problem will be even further complicated by the general inability of hydrate formation within a pipeline to reach thermodynamic equilibrium due to restrictions imposed by either the Gibbs phase rule or transport limitations. Consider a simple case of methane hydrate forming from water present in methane; here C , the number of components is two (water and methane), and the number of phases, N , is two phases as well (solid hydrate and methane gas with impurities). According to the Gibbs phase rule ($F = C - N + 2$), this will leave two degrees of freedom, *i.e.* $F = 2$. Though this result would appear to indicate a chance for the system to achieve equilibrium by varying local temperature and pressure hydrate nucleus might never reach a critical size due to mass transport limitations and very low concentration of water in methane. Getting rid of crystallization heat will pose yet another issue that can severely limit the rate of hydrate formation, since methane is a much worse thermal conductor compared to hydrate and liquid water clusters prior to hydrate formation.

The presence of solid surfaces will also have an indirect effect on hydrate formation on the interface between the methane-rich gas and the aqueous phase adsorbed on rusty walls. This potential impact of water-wetting surfaces on the phase transitions should not be discounted just because of the gas phase will dominate as far as the mass is concerned. Hydrate nucleation and growth may occur when either **both** water and hydrate guest molecules are adsorbed on the surface or only water is in the adsorbed phase and guest molecules species are imported from the methane-rich phase. Given the general lack of equilibrium, chemical potentials of hydrate-forming species will not be the same across the phases. In accordance with statistical thermodynamics hydrate

models of¹, this will lead to formation of several different co-existing hydrate phases even in the simple case of only water present in methane. Mixtures of ethane and methane will form structure I hydrates due to the very favorable stabilization of the large cavity by ethane. Additional content of propane is likely to lead to a mixed hydrate since structure will be favorable as long as propane is left in the gas mixture. Subsequent hydrate formation for remaining ethane and methane will be structure I.

Different Hydrate Formation Routes: Impact Of Multiple Phases

Table 1 lists the alternative routes to hydrate formation and re-dissociation relevant for pipeline transport of natural gas analyzed and ranked basing on their associated free energy changes:

$$\Delta G_i = \delta \left[x_w^{H,i} (\mu_w^{H,i} - \mu_w^p) + x_{gas}^{H,i} (\mu_{gas}^{H,i} - \mu_{gas}^p) \right] \quad (1)$$

Subscript “w” stands for “water” in either hydrate or other phase, “gas” for hydrate guest molecules; *H* is for hydrate phase, “*i*” indicates the scenario, “*p*” refers to either liquid, gas or adsorbed phase, *x* is composition, μ , chemical potential. Sign δ is 1 for hydrate formation or reformation and -1 for dissociation. As pointed out earlier, the different pathways of Table 1 will lead to creation of hydrate varying in filling fraction and thus free energy, i.e. its own individual hydrate phase.

When there are only two components (methane and water) involved, and the number of possible phases exceeds two, as it will for pipeline transport with four phases (methane-rich fluid, aqueous phase, adsorbed phase, hydrates), the Gibbs phase rule will correspond to a system over-determined by two parameters. It might seem that adding more components, like ethane and/or propane, to the fluid phase would increase the number of degrees of freedom and make equilibrium attainable. From the dynamic point of view, it is however unlikely that hydrate equilibrium can be reached during pipeline transport of natural gas with impurities. One should keep in mind that thermodynamics will guide the system towards the lowest free energy state currently possible via driving forces proportional to the free energy differences. These forces will be fairly large in our case and resulting in more stable hydrates forming first and hydrate composition changing in time. While a stable hydrate are prevented from reforming into a less stable form, a less stable hydrate is unable to reform into a more stable one without a supply of new hydrate formers. Under continuous flow, the latter option may become feasible due to continuous supply of “fresh” components from the stream. In addition, when in contact with phases under-saturated with respect to hydrate formers, hydrate may dissolve or reform with different compositions.

Scenarios covered by conventional industrial hydrate risk evaluation schemes largely assume that hydrate will nucleate and grow from gas and liquid water (route 6). We are not aware of any available commercial or academic codes that consider homogeneous hydrate formation from hydrate guest components dissolved in water. And no hydrate code available at present is able to treat heterogeneous hydrate formation in the presence of solid surfaces. Given the growing body of evidence that growth and propagation of thin hydrate films on the interfaces will be impacted by hydrate formation towards surfaces even in stationary situations, ignoring these processes can constitute a serious oversight. We believe that this work will also contribute to stimulating the discussion on how to incorporate these aspects^{2,3} into a new generation of hydrate risk evaluation tools based on non-equilibrium thermodynamics. The outlined approach can also be extended to other hydrate-forming fluids containing water, including transport of liquid hydrocarbons containing structure I and II hydrate formers. In general, the proposed analysis scheme can also include guest components that form structure H hydrates, although kinetic studies seems to indicate that structure H forms slowly compared to structure I and II.

The various possible hydrate phase transitions listed in table 1 is not even complete but at least provides a flavor of the complexity of competing hydrate phase transitions in a general non-equilibrium situation. Given all of the possibilities listed in Table 1, a truly rigorous approach to hydrate risk evaluation would be the one that incorporates mass and heat transport as constraints inside a free energy minimization scheme that also accounts for hydrodynamic effects. A simpler (but less rigorous) analysis scheme more compatible with conventional hydrate equilibrium codes can provide a viable alternative when consistent absolute thermodynamic properties are available for the different phase transitions. One may apply either the classical nucleation theory or the Multi-component Diffuse Interface Theory (MDIT)^{2,4} to evaluate the phase transitions in Table 1. Routes 1 through 4 can be excluded from consideration immediately since their corresponding free energy changes will be either positive or not negative enough to overcome the penalty of the surroundings work. Simple kinetic theories can be used to eliminate very slow phase transitions and thus focus the evaluation on a handful of truly important ones.

One of the main goals in this work involved presenting routes to absolute thermodynamic properties (i.e. with ideal gas as reference state) for all the co-existing. A section focusing on equilibrium thermodynamics that follows outlines approaches and models we have used for this purpose. While the models employed there may be refined and extended, the approach presented provides a good starting point for an accurate analysis of

hydrate formation. We then briefly discuss the consequences of the non-equilibrium nature of hydrate phase transitions. The subsequent sections describe our numeric simulations; they are centered on assessing the possible hydrate formation routes with the aid of equation (1) and absolute thermodynamics. It should be pointed out that absolute thermodynamic properties obtained from atomistic simulations have been quite successful at predicting hydrate equilibrium curves^{1,2}.

Table 1. Some of the various possible routes to formation and dissociation of natural gas hydrate. δ is the sign of free energy change involved in hydrate phase transition, in which value 1 indicates favorable formation and -1 dissociation. i is just a phase transition index.

i	δ	Initial phase(s)	Driving force	Final phase(s)
1	-1	Hydrate	Outside stability in terms of local P and/or T	Gas, Liquid water
2	-1	Hydrate	Sublimation (gas under saturated with water)	Gas
3	-1	Hydrate	Outside liquid water under saturated with respect to methane and/or other enclathrated impurities originating from the methane phase	Liquid water, (Gas)
4	-1	Hydrate	Hydrate gets in contact with solid walls at which adsorbed water have lower chemical potential than hydrate water	Liquid water, Gas
5	+1	Gas/fluid	Hydrate more stable than water and hydrate formers in the fluid phase	Hydrate
6	+1	Gas + Liquid water	Hydrate more stable than condensed water and hydrate formers from gas/fluid	Hydrate
7	+1	Surface reformation	Non-uniform hydrate rearranges due to mass limitations (lower free energy hydrate particles consumes mass from hydrates of higher free energy)	Hydrate
8	+1	Aqueous phase	Liquid water super saturated with methane and/or other hydrate formers, with reference to hydrate free energy	Hydrate
9	+1	Adsorbed	Adsorbed water on rust forms hydrate with adsorbed hydrate formers	Hydrate
10	+1	Adsorbed + fluid	Water and hydrate formers from gas/fluid forms hydrate	Hydrate

Equilibrium Thermodynamics Of Fluid

A thermodynamic equilibrium is achieved when temperatures, pressures and chemical potentials of all components are equal in all co-existing phases. To insure the same reference values for free energy, all the chemical potential estimates, no matter what the phase, should employ ideal gas as the reference state:

$$\mu_i(T, P, \bar{y}) - \mu_i^{\text{ideal gas}}(T, P, \bar{y}) = RT \ln \phi_i(T, P, \bar{y}) \quad (2)$$

where ϕ_i is the fugacity coefficient of component i in a given phase.

Another reference state for the chemical potential of a liquid state component i may also be used as an intermediate:

$$\mu_i(T, P, \bar{x}) - \mu_i^{\text{idealliquid}}(T, P, \bar{x}) = RT \ln \gamma_i(T, P, \bar{x}) \quad (3)$$

$$\lim(\gamma_i) = 1.0 \quad \text{when } x_i \rightarrow 1.0$$

where γ_i is the activity coefficient for component i in the liquid mixture. Note that when chemical potential of pure water has been estimated using molecular simulations, the application of equation (3) in case of water will be also based on absolute thermodynamics. The data from Kvamme & Tanaka¹ will be used in this work.

Infinite dilution is yet another reference state that has proven useful in case of gases with low solubility in water (route 8):

$$\mu_i(T, P, \bar{x}) - \mu_i^\infty(T, P, \bar{x}) = RT \ln \left[x_i \gamma_i^\infty(T, P, \bar{x}) \right] \quad (4)$$

$$\lim(\gamma_i^\infty) = 1.0 \quad \text{when } x_i \rightarrow 0$$

with superscript “ ∞ ” standing for infinite dilution. This particular convention is known as the non-symmetric convention since the limit of the activity coefficient for the component i will approach unity as its

mole fraction vanishes. As shown in ^{4,5}, molecular dynamics combined with the Gibbs-Duhem relation provides a convenient method to estimate absolute values for the required chemical potential at infinite dilution.

Provided that thermodynamic properties of all phases can be defined and evaluated both in equilibrium and outside of it, the combined first and second laws of thermodynamics would enforce a certain partitioning of all available components (and the total mass) over all phases able to coexist under local pressure and temperature conditions. The estimation of out-of-equilibrium values will be fairly straightforward for most of the relevant fluid phases, with only the hydrate phase requiring a special consideration (see extensive discussion in Kvamme *et al*²). Combining thermodynamic formulations for fluids in equations (2) to (4) with hydrate non-equilibrium formulations from Kvamme *et al*² will make it fairly straightforward to minimize the free energy and obtain estimates for the local phase concentrations that satisfy the first and the second law of thermodynamics. Several algorithms capable of implementing this approach are available in the open literature.

Except in the case of hydrates, relevant pressures and temperatures will largely correspond to a liquid state. Cases and scenarios considered here entail very limited mutual solubilities and/or limited concentrations, especially that of water in methane. The following approximation should therefore prove sufficiently accurate for most industrial applications in which hydrate formation is a risk factor:

$$\mu_{i,j}(T, P, \vec{x}) \approx \mu_{i,j}^{\infty}(T, P) + RT \ln \left[x_{i,j} \gamma_{i,j}^{\infty}(T, P, \vec{x}) \right] \quad (5)$$

where subscript j refers to components; subscript i denotes different phases. In the context of this work, j is “methane” in case of the methane-rich phase and “H₂O” for the aqueous phase, “ ∞ ” refers to infinite dilution.

Equilibrium Thermodynamics Of Hydrate

Chemical potential of water when in the hydrate phase can be found by applying the statistical mechanical model for water in hydrate ¹:

$$\mu_{w,H} = \mu_{w,H}^0 - \sum_{k=1,2} RT v_k \ln \left(1 + \sum_i h_{ik} \right) \quad (6)$$

where subscript H denotes the hydrate phase, superscript 0 stands for the empty hydrate structure; v_k is the fraction of cavity of type k per water molecule. In case of structure I hydrates; $v_k = 1/23$ for small cavities (20 water molecules) and $3/23$ for large cavities (24 water molecules). h_{ik} is the canonical partition function for a cavity of type k containing a “guest” molecule of type i , given by the following equation:

$$h_{ik} = e^{\beta(\mu_i^H - \Delta g_{ik}^{inc})} \quad (7)$$

where β is the inverse of the gas constant times temperature, while Δg_{jk}^{inc} reflects the impact on hydrate water from the inclusion of the “guest” molecule i in the cavity ¹. At equilibrium, chemical potential of

hydrate guest molecule i , μ_i^H , must to be identical to its chemical potential in the phase it has been extracted from. The hydrate content of all guest gas components can be estimated by applying equation (4) to calculate their chemical potential when dissolved in the methane phase. It must be noted that chemical potential of liquid water will be influenced by the presence of hydrogen sulfide and carbon dioxide while the solubility of hydrocarbons in liquid water is so low that they might be approximated to not affect activity of liquid water. Since water will totally dominate the dew point location, a simple approximation for hydrate formation in case of liquid water dropout (*i.e.* route 6) can be achieved by applying equation (8) below. Solving equation (8) for the given local temperature will yield the corresponding hydrate formation pressure. If this formation pressure is lower than the local pressure defined by flow’s fluid dynamics, one can then estimate the mole fractions of condensed water by simultaneously satisfying the mass balance and equilibrium criteria. This approach is quite similar to flash calculations commonly employed in chemical engineering, though in terms of fugacity formulation rather than a chemical potential one.

$$\mu_w^{0,H} - \sum_{k=1,2} RT v_k \ln \left(1 + \sum_i h_{ik} \right) = \mu_{i,H_2O}^{purewater}(T, P) + RT \ln \left[x_{i,H_2O} \gamma_{i,H_2O}(T, P, \vec{x}) \right] \quad (8)$$

We should emphasize here that chemical potential of empty hydrate structure estimated from Kvamme & Tanaka ¹ has been verified to have predictive capabilities, which makes any empirical

formulations redundant and even possibly non-physical, given the fundamental nature of chemical potential. If the estimated hydrate formation pressure is lower than the local one, hydrate will form via this particular route.

A subsequent flash calculation using local pressure and temperature will provide the upper limit of liquid water mole fraction that can be supported by the methane-rich phase. If water dew-point pressure is lower than the local pressure, water will drop out as a liquid phase. In this case, one may assume that free water will be available for the process of hydrate formation, with hydrate of lowest free energy appearing first. Given that ethane and propane is a more vigorous hydrate former than methane, the initially formed hydrates will be much richer in ethane and propane compared to any later ones. In contrast to the “standard” calculations, this approach does not consider the usual hydrate formation from the “bulk” but rather searches for hydrate with the lowest absolute free energy able to nucleate from the available natural gas mixture under the kinetic restrictions of mass- and heat transport. In other words, one would aim to minimize the following equation in terms of hydrate formation pressure while taking into account the fact our system will be unable to reach equilibrium:

$$G^H = \sum_i x_i^H \mu_i^H \quad (9)$$

One can apply the non-equilibrium description of hydrate due to Kvamme *et al.*² to follow the free energy gradients until the methane phase has been mostly depleted of the best hydrate former, ethane/propane. The analysis of equation (9) will also require the knowledge of hydrate composition, which can be found by applying statistical thermodynamic theory to the adsorption hydrate model (left hand side of equation (8)); the composition will be given by:

$$\theta_{ik} = \frac{x_{ik}^H}{v_k (1 - x_T)} = \frac{h_{ik}}{1 + \sum_i h_{ik}} \quad (10)$$

where θ_{ik} is the filling fraction of component i in cavity type k , x_{ik}^H is the mole fraction of component i in cavity type k , x_T is the total mole fraction of all guests in the hydrate, and v_k is, as defined above, the fraction of cavities per water of type k .

We have fitted computed free energies of guest inclusion in the large cavity of structure I to a series in inverse reduced temperature.

$$\Delta g^{inclusion} = \sum_{i=0}^5 k_0 \left[\frac{T_c}{T} \right]^i \quad (11),$$

where T_c is the critical temperature of the guest molecule in question (see figures 1 and 2).

The free energy of inclusion in equation (11) can be estimated following Kvamme & Tanaka¹ and Kvamme *et al.*⁵ for the components included in this study (methane, Ethane and Propane). Thermodynamic consistency has been a high priority throughout this work, and it was not our intention to adjust any parameters to fit experimental data. Molecular dynamics simulations reported in this work were meant to extend the approach of¹ to larger hydrate systems and temperatures ranging between 273.15 K and 280 K. This was done in order to get a better resolution in the range of interest for this study. The main focus of our efforts was to study hydrate risks during transport of natural gas between Norway and the continent (Germany) via the North Sea pipelines.

The seafloor temperatures there rarely rise above 6°C. Figures 1 and 2 shows plots of the parameters applied as function of temperature. Parameters corresponding to empty hydrates and ice will not be significantly affected, allowing the parameters of Kvamme & Tanaka¹ to be used. Similarly, chemical potential estimates for liquid water were extended from 0°C by means of thermodynamic relationships and experimental data on enthalpy of dissociation and liquid water heat capacities. See Kvamme & Tanaka¹ for more details.

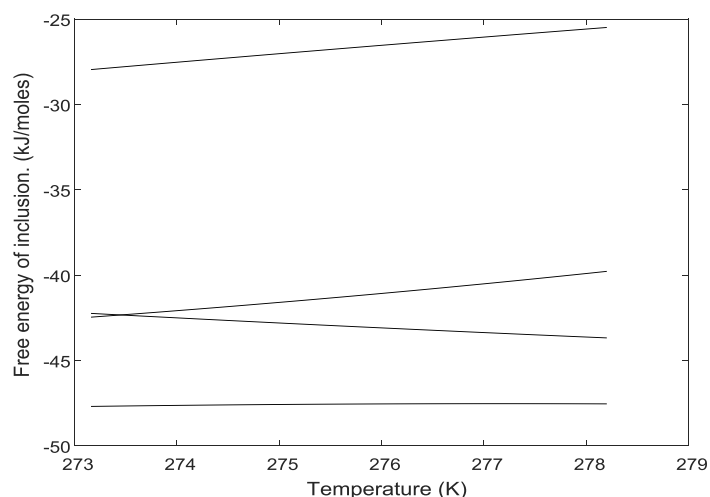


Figure 1. Free energy of inclusion of guest into hydrate structure II cavities (as positioned at 278 K). Lower curve is for propane in large cavity followed by ethane in large cavity and then methane in large cavity and then on top methane in small cavity.

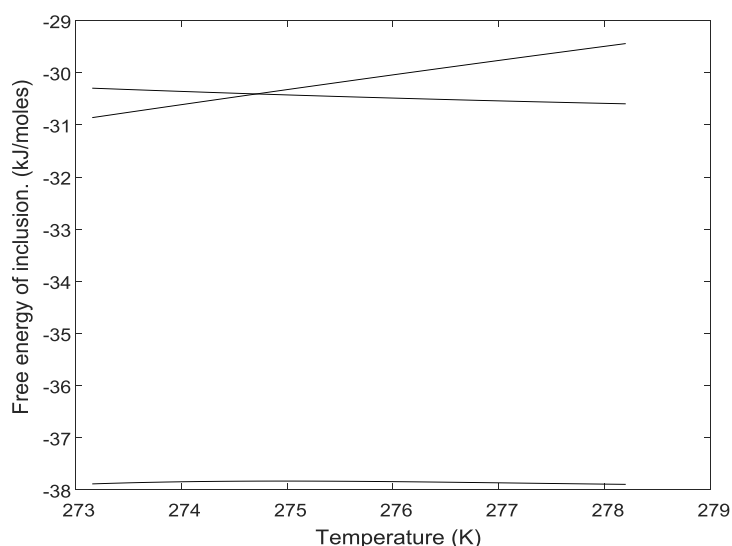


Figure 2. Free energy of inclusion of guest into hydrate structure I cavities (as positioned at 278 K). Lower curve is for ethane in large cavity followed by methane in small cavity and then methane in large cavity on top.

Verification Of Models And Other Assumptions

Since the free energies of guest molecule inclusions in equation (7) are based on molecular simulations of model systems we do not expect the resulting pressure, temperature equilibrium curves to match experimental data. But rather than making empirical fitting functions it is better in the context of this paper to stick to the values obtained and as plotted in figures 1 and 2 above.

Comparison for structure I hydrate of methane (figure 3) and ethane (figure 4) with experimental values show a fair agreement while structure II estimates for propane (figure 5) is underestimated in terms of stabilization. But they are nevertheless demonstrating that the model systems are suitable for qualitative evaluation of water drop out curves. It is also important to keep in mind that, as consequence of the first and second laws of thermodynamics, mixed hydrates will frequently occur. Like for instance in the system of 90% methane and rest ethane. Since this system will form structure I, and large cavities suitable for ethane are in a ratio of 3:1 versus small cavities, then it is clear that the first hydrates that forms will be very rich in ethane and the final hydrates will be methane. So within the scope of this work also estimates for that system is deemed sufficient. Possible users of the findings in this work can easily incorporate our models into their own hydrate codes. Very limited experimental data for the gas mixture hydrate consisting of methane, ethane and propane were found in open literature. For a system of 10% ethane in methane the estimated equilibrium curve is plotted

along with experimental data in figure 6. Given the limited amount of ethane in the system and a 3:1 ratio of large to small cavities in structure I it is expected that hydrate from this system in reality is a mixture of various hydrates ranging from an initial ethane rich hydrate to a final methane hydrate.

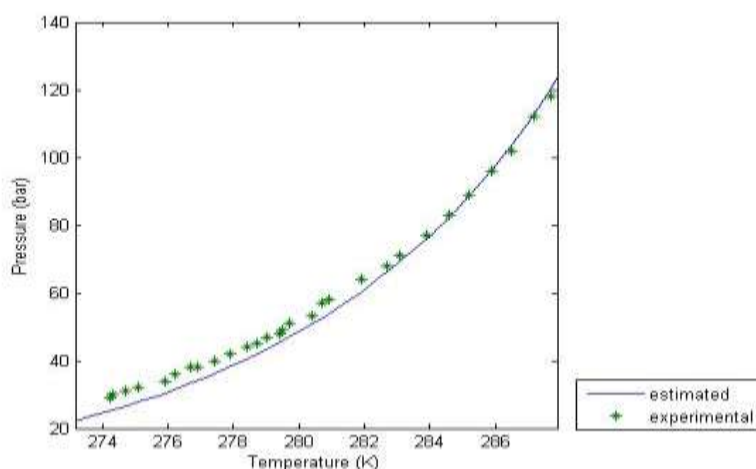


Figure 3. Estimated and experimental hydrate equilibrium curve for pure methane. Solid line – our estimates; asterisks – experimental data from Maekava⁶.

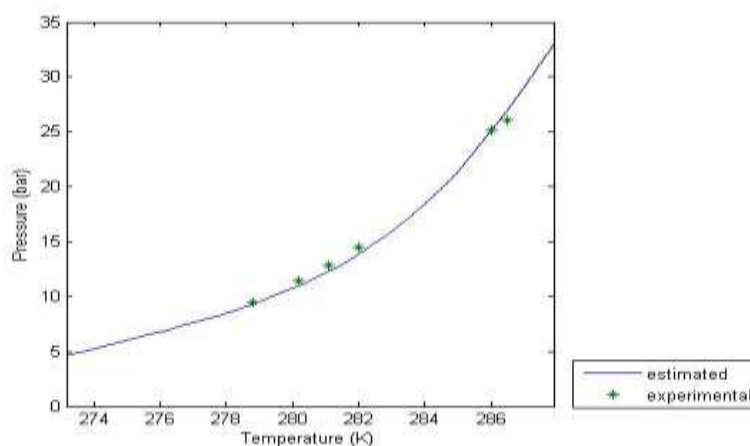


Figure 4. Estimated and experimental hydrate equilibrium curve for pure ethane. Solid line – our estimates; asterisks – experimental data from Holder and Hand⁷.

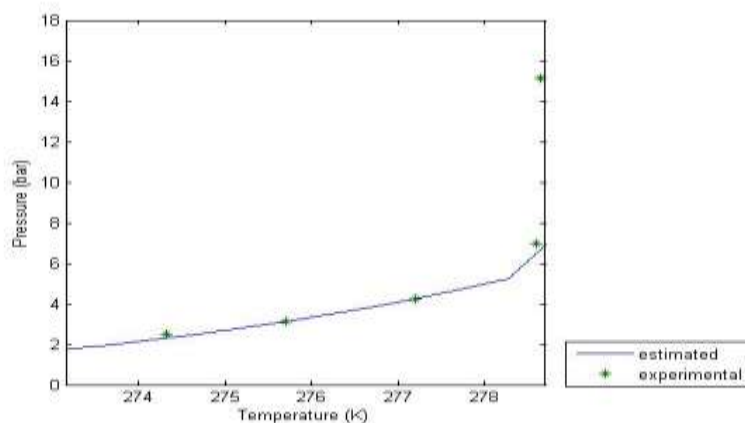


Figure 5. Estimated and experimental hydrate equilibrium curve for pure propane. Solid line – our estimates; asterisks – experimental data from Reamer *et al*⁸.

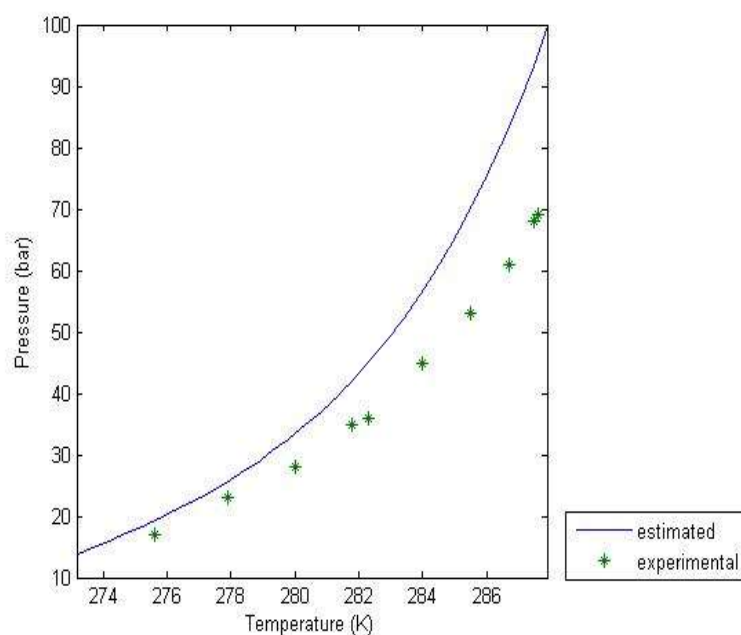


Figure 6. Estimated and experimental hydrate equilibrium curve for a mixture of 90% methane and 10% ethane. Solid line – our estimates; asterisks – experimental data from Maekava⁶.

Analysis Of Routes To Hydrate Formation

The primary goal of this study was to gain insights into possible routes to hydrate formation and their relative importance during pipeline transport of natural gas, and also investigate how ethane and propane will influence the hydrate formation. In terms of the possible hydrate phase transitions listed in table 1, a conservative approach to hydrate risk evaluation would disregard all routes resulting in re-dissociation of hydrate (*i.e.* routes 1 – 4). The focus of this study was to investigate routes 6 and 10 and they are discussed below.

Hydrate formation involving condensed water and hydrate formers from the natural gas stream (routes 6)

Combining equation (3) for water in the condensed liquid phase with pure water in the ideal liquid water term from Kvamme & Tanaka¹ with residual thermodynamics (equation (2)) for water dissolved in natural gas will yield an approximate of water dew-point concentration for water in natural gas at given T and P. The above-described scheme might suffice for risk analysis related to route 6. Alternatively, combined mass balances and equilibrium can be solved iteratively for liquid water drop-out and water phase composition. If hydrate formation conditions are met, hydrate will form. Equation (2) with SRK⁹ has been used as the equation of state for all components and natural gas mixtures. SRK is deemed accurate enough for the purposes of illustration. The SRK equation⁹ was used to evaluate the deviations from ideal gas behavior via the fugacity coefficient.

While 50 bars may be a typical pressure during gas processing 250 bars is typical during pipeline transport. Seafloor temperatures in the North Sea are typically between -1 degrees Celsius and 6 degrees Celsius. Figures 7 to 9 shows plots of limits for water content before drop out as liquid. This is actually water dew-point curves under the simplification that the initial theoretical droplet is pure water. Due to the low density of methane (figure 7) at all conditions as compared to ethane and propane (figures 8 and 9 respectively) densities at same conditions there is a qualitative change.

For methane the water solubility decrease with increasing pressure while the opposite is the case for ethane and propane, which have substantially higher density for the high pressure and would make it more difficult for water to enter.

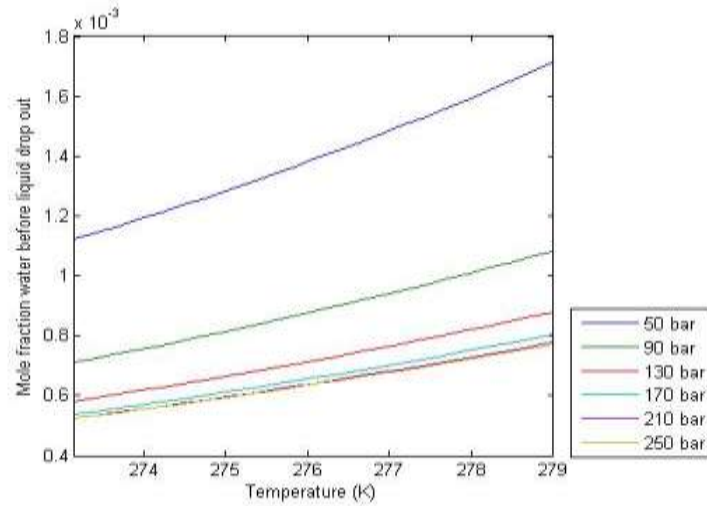


Figure 7. Maximum water content before liquid water drop out, for pure methane. Curves from top to bottom correspond to pressure 50 bar, 90 bar, 130 bar, 170 bar, 210 bar, 250 bar.

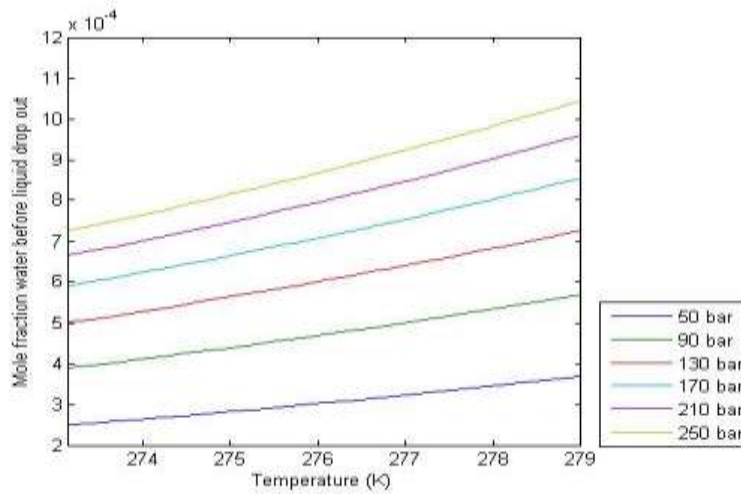


Figure 8. Maximum water content before liquid water drop out, for pure ethane. Curves from top to bottom correspond to pressure 250 bar, 210 bar, 170 bar, 130 bar, 90 bar, 50 bar.

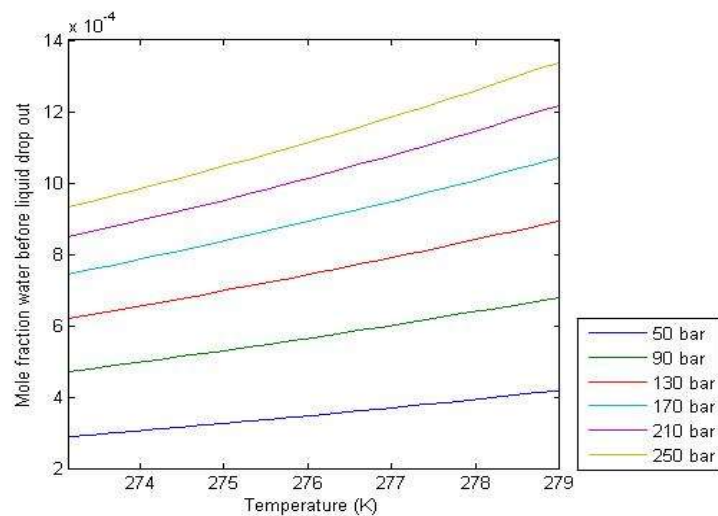


Figure 9. Maximum water content before liquid water drop out, for pure propane. Curves from top to bottom correspond to pressure 250 bar, 210 bar, 170 bar, 130 bar, 90 bar, 50 bar.

Natural gas mixtures are dominated by methane and some realistic mixtures are examined in figures 10 – 13. Although there are some differences in the behavior in terms of maximum water content before drop-out as liquid the trend is similar to that for pure methane in figure 7 although shifted slightly towards lower values for pressures up to 130 bars.

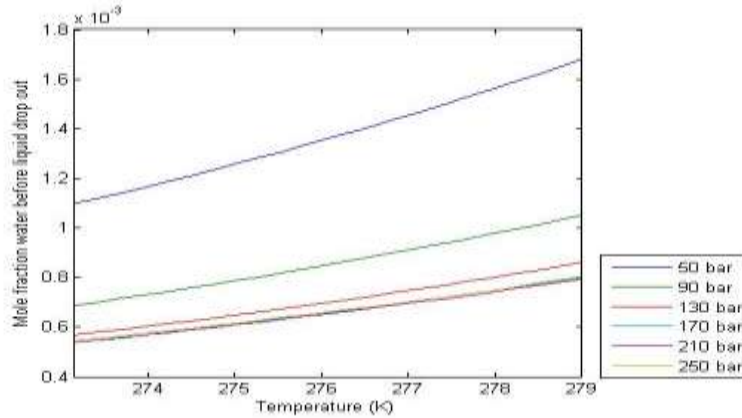


Figure 10. Maximum water content before liquid water drop out, for a mixture of 90% methane and 10% ethane. Curves from top to bottom correspond to pressure 50 bar, 90 bar, 130 bar, 170 bar, 210 bar, 250 bar.

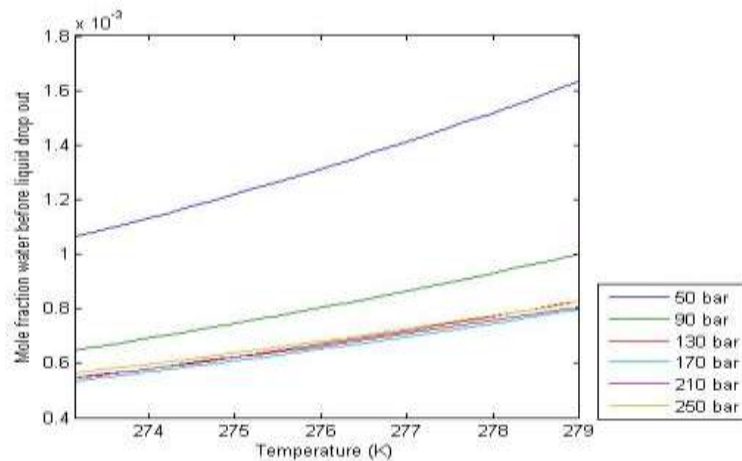


Figure 11. Maximum water content before liquid water drop out, for a mixture of 80% methane and 20% ethane. Curves from top to bottom correspond to pressure 50 bar, 90 bar, 130 bar, 170 bar, 210 bar, 250 bar.

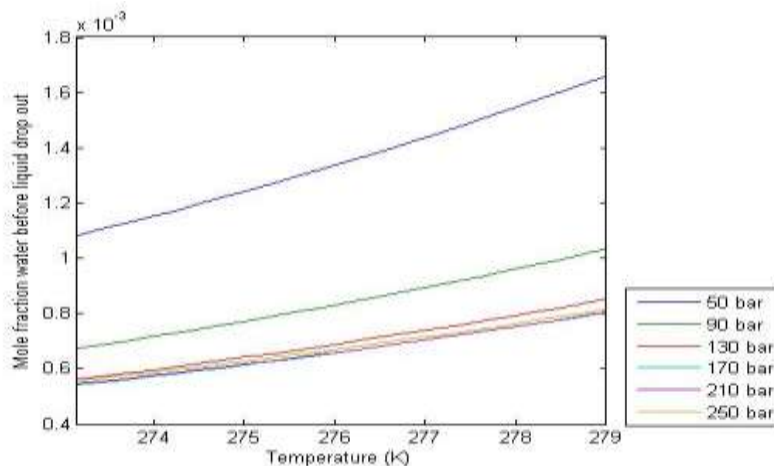


Figure 12. Maximum water content before liquid water drop out, for a mixture of 90% methane and 10% propane. Curves from top to bottom correspond to pressure 50 bar, 90 bar, 130 bar, 170 bar, 210 bar, 250 bar.

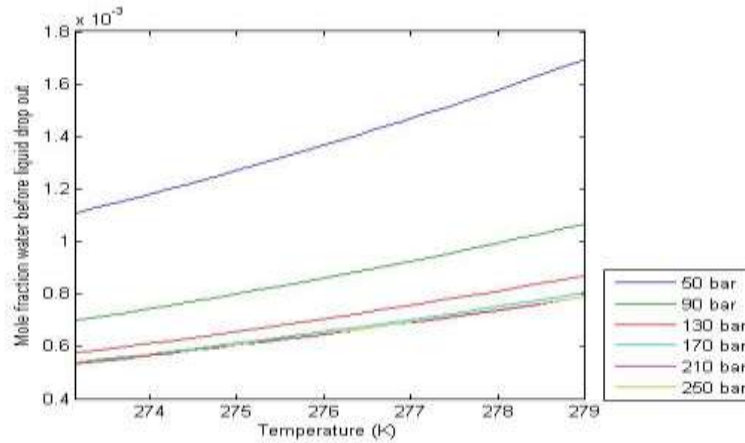


Figure 13. Maximum water content before liquid water drop out, for a mixture of 95% methane, 4% ethane and 1% propane. Curves from top to bottom correspond to pressure 50 bar, 90 bar, 130 bar, 170 bar, 210 bar, 250 bar.

Hydrate formation involving adsorbed water and hydrate formers from the fluid stream(route 10)

The maximum water content before drop-out as adsorbed on Hematite is plotted for methane, ethane and propane in figures 14, 15 and 16 respectively. The general trend is the same as for the water dew-point mole-fraction in the previous section but the actual limits are far smaller – in the order of 1/20 as compared to the water dew-point criteria.

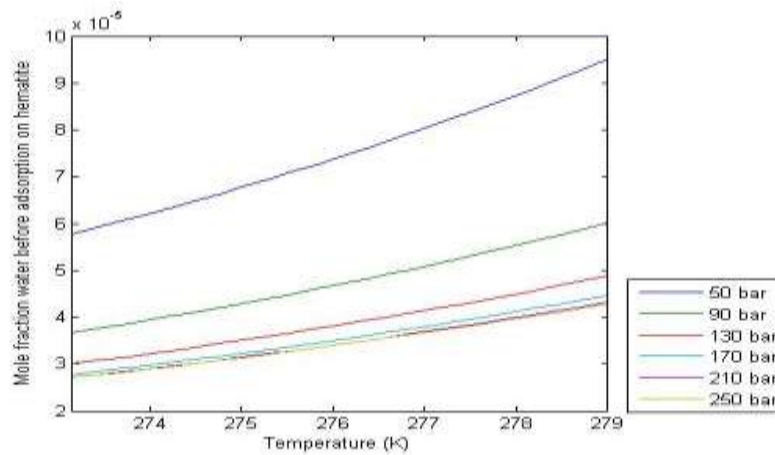


Figure 14. Maximum water content before adsorption on hematite, for pure methane as carrier gas. Curves from top to bottom correspond to pressure 50 bar, 90 bar, 130 bar, 170 bar, 210 bar, 250 bar.

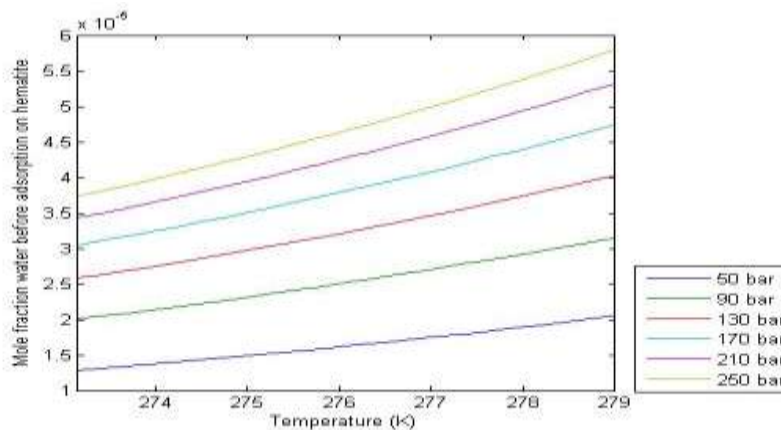


Figure 15. Maximum water content before adsorption on hematite, for pure ethane as carrier gas. Curves from top to bottom correspond to pressure 250 bar, 210 bar, 170 bar, 130 bar, 90 bar, 50 bar.

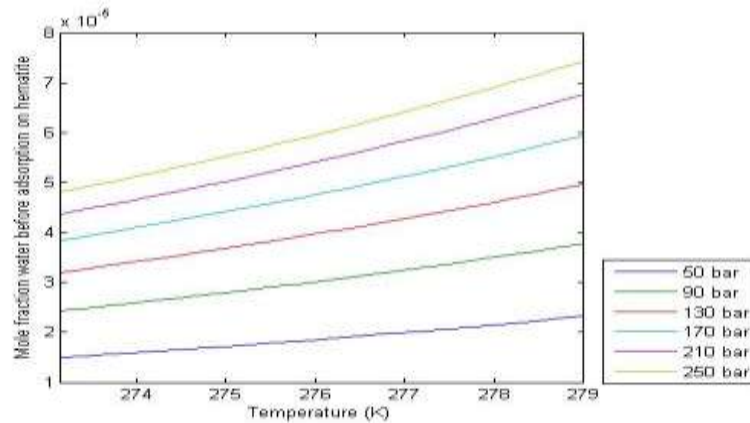


Figure 16.Maximum water content before adsorption on hematite, for pure propane. Curves from top to bottom correspond to pressure 250 bar, 210 bar, 170 bar, 130 bar, 90 bar, 50 bar.

Examining the same natural gas mixtures as in the previous section the trend is as expected still dominated by methane but the tolerance limits for water mole-fractions are shifted dramatically as compared to the water dew-point criteria, as can be seen from the plots in figures 17 – 20.

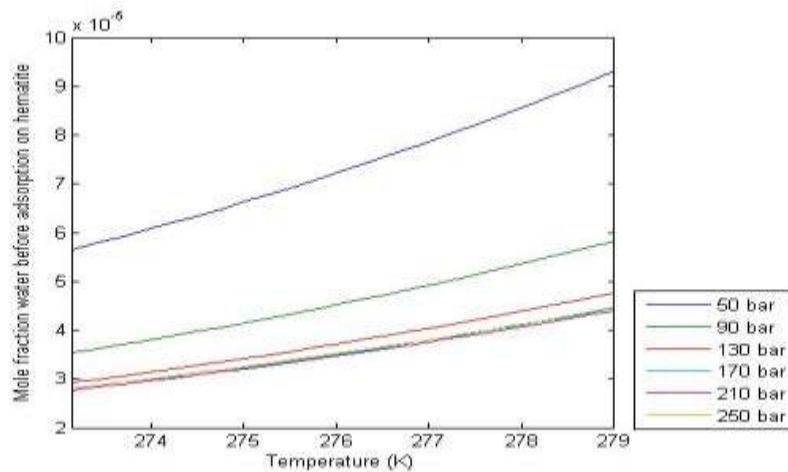


Figure 17.Maximum water content before adsorption on hematite, for a mixture of 90% methane and 10% ethane. Curves from top to bottom correspond to pressure 50 bar, 90 bar, 130 bar, 170 bar, 210 bar, 250 bar.

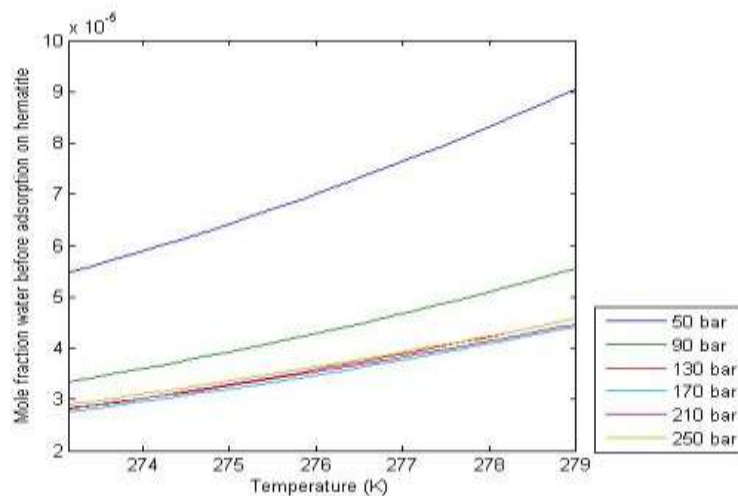


Figure 18.Maximum water content before adsorption on hematite, for a mixture of 80% methane and 20% ethane. Curves from top to bottom correspond to pressure 50 bar, 90 bar, 130 bar, 170 bar, 210 bar, 250 bar.

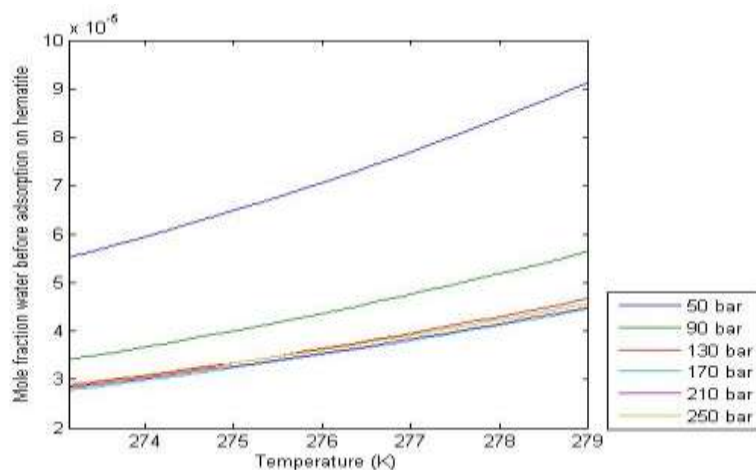


Figure 19.Maximum water content before adsorption on hematite, for a mixture of 90% methane and 10% propane. Curves from top to bottom correspond to pressure 50 bar, 90 bar, 130 bar, 170 bar, 210 bar, 250 bar.

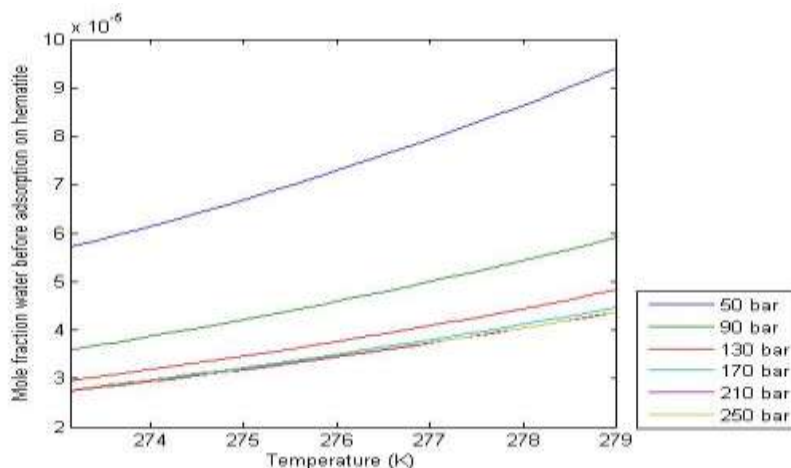


Figure 20.Maximum water content before adsorption on hematite, for a mixture of 95% methane, 4% ethane and 1% propane. Curves from top to bottom correspond to pressure 50 bar, 90 bar, 130 bar, 170 bar, 210 bar, 250 bar.

The main difference between route 10 and route 6 is the concentration at which water drops out from the gas. Hydrate formation according to route 10 is only possible at some distance from the rust surface since water chemical potential in the adsorbed layer will be too low to form hydrates. Our earlier Molecular Dynamics simulations¹⁰ have shown that adsorbed water structure will strongly affect the liquid water until about 3 – 4 molecular diameters from hematite surface. A structured water film roughly 1.2 nm in thickness will form on the hematite surface and bridge it with the hydrate hematite surface. This formation of interface hydrate from bulk liquid water and hydrate formers from the gas phase will be the common feature for routes 6 and 10. Adsorbed water chemical potential as low as 3.4 kJ/mole less than liquid water chemical potential make a big difference in limits for water drop-out mole-fractions.

Figures 14 through 20 show the estimated upper water content supported by the natural gas mixtures before it starts dropping out via adsorption on hematite for pure methane, ethane and propane, and also a variety of mixtures of these. This includes a mixture of 95% methane, 4% ethane and 1% propane, which is comparable to the Troll composition¹¹. The trend for maximum water tolerance remains the same as in the case of water dew-point but shifted 1 to 2 orders of magnitude downwards.

The Consequences Of Non-Equilibrium Thermodynamics

The non-equilibrium aspects of hydrate phase transitions discussed above will impose substantial challenges for laboratory experiments conducted at temperatures and pressures falling with the hydrate stability regions. While methane solubility in water is so small that one can safely ignore any hydrate implications, the situation will be very different in case of impurities like ethane and propane. This will be due to ethane and propane solubility being largely controlled by the presence of hydrate phases. Within the hydrate stability

region where water exists as hydrate, chemical potential of water encaging hydrate guest molecules will be lower than that of liquid water at the same temperature and pressure. Hence, the solubility of ethane and propane will be significantly smaller for a similar system that does not contain hydrate. This fact can be verified by a limited-range extrapolation of the rigorous version of Henry's law into the hydrate region. The difference between the hydrate-controlled maximum concentration of ethane and propane in water and the ethane and propane dissolved in water will correspond to the amount of hydrate that can be produced from ethane and propane dissolved in water^{2,4}

The impact of solid surfaces will introduce additional challenges when it comes to interpretation of experimental results. We are not aware of any experiments that attempted to quantify the impact of solid water-wetting surfaces on carbon dioxide solubility in hydrate-controlled regions. Given the arguments presented above, even the most recent experiments on carbon dioxide solubility in hydrate-forming regions may still be subject to misinterpretation, leaving many of estimates presented in this work without experimental data to comparison to. Hydrate nucleation and growth under non-equilibrium conditions will be facilitated by heterogeneous nucleation (solid surfaces and hydrate former/water surface), and since chemical potentials of hydrate formers and water may differ from the bulk phase properties, the composition and free energy of formed hydrates will be different as well. Different experimental facilities with varying materials and set-ups that give rise to variations in the progresses of hydrate formation will impose additional uncertainties.

The challenge of non-equilibrium thermodynamics and competing hydrate phase transitions can be handled on several levels, a number of strategies discussed elsewhere (see^{2,3} and references therein). These discussions can be supplemented by corresponding equations for hydrate sub- and super- saturation presented in this paper. The simplified discrete evaluation scheme outlined here can easily be implemented to extend the existing industrial hydrate risk evaluation codes by enumerating possible routes this will yield corresponding levels of acceptable carbon dioxide content. The rigorous schemes of^{2,3} do require consistent reference values for thermodynamics of all phases interacting with the hydrate. Estimates based on routes 6 or 10 are conservative since no routes of hydrate dissociation have been accounted for. This can be accomplished through advanced modeling on nano to millimeter scale using Phase Field Theory (PFT)^{12, 13}. Due to the low concentrations of water and possible resolutions in Computational Fluid Dynamics (CFD) simulations it is more unclear if a similar analysis is as feasible within CFD. But a conservative approach as demonstrated here is certainly feasible to implement in CFD tools.

II. CONCLUSIONS

Our rigorous analysis of the Gibbs phase rule applied together with the first and the second laws of thermodynamics has proven that hydrate nucleation and growth during transport of methane-rich gas with water and other impurities is extremely unlikely to attain equilibrium. Instead, the time evolution of phase transitions will be governed by the free energy minimum. The corresponding thermodynamic analysis of phase transitions will require knowledge of consistent thermodynamic properties for all components in all the phases. In this work, we have shown the way to calculate the chemical potential for water in all phases, including empty hydrate, adsorbed phase, and aqueous solution by plugging properties yielded by molecular dynamics simulations into classical thermodynamic relationships. The most likely hydrate formation scenario will involve water dropping out via adsorption onto rusty pipeline walls. The hydrate formation will start from the accumulated water film. In a possible revision of current best practices for hydrate prevention, it is therefore recommended to reduce water level in the methane-rich phase to below the concentration triggering adsorption-dominated drop-out. Calculating this level will require a procedure similar to that of water dew-point estimation but using chemical potential values characteristic for adsorption on the surface of interest (either hematite as in this work, or other iron oxide/hydroxide and iron carbonates). It is, however, important to point out that possible hydrate nucleating towards rusty surfaces are unable to attach directly to these iron oxide surfaces due to incompatibility of partial charges between hydrate water partial charges and partial charges on atoms in the mineral. These hydrate nuclei will be linked by structured water to the iron oxides but might be released by frictional forces induced by flow. As such continued hydrate growth can happen towards the iron oxide walls or in the hydrocarbon flowstream by attracting more water and hydrate formers from the hydrocarbon stream, or dissolving again if the local hydrocarbon composition is under saturated with water.

ACKNOWLEDGEMENTS

We acknowledge the grant and support from Research Council of Norway through the project "FME-SUCCESS". Support from TOTAL, Gassco and Research Council of Norway through the project "CO2/H2O+" is also greatly acknowledged.

REFERENCES

- [1]. B. Kvamme, H. Tanaka, "Thermodynamic Stability of Hydrates for Ethane, Ethylene, and Carbon Dioxide," *J. Phys. Chem.*, Vol. 99, PP. 7114-7119, 1995.
- [2]. B. Kvamme, T. Kuznetsova, P.-H. Kivelæ, J. Bauman, "Can hydrate form in carbon dioxide from dissolved water," *PCCP*, Vol. 15, PP. 2063-2074, 2013.
- [3]. T. Buanes, "Mean-field approaches applied to hydrate phase transition kinetics," PhD thesis, University of Bergen, Norway, 2008.
- [4]. B. Kvamme, T. Kuznetsova, S. Stensholt, S. Sjøblom, "Investigating chemical potential of water and H₂S in CO₂ streams using molecular dynamics simulations and the Gibbs-Duhem relation," *J. Chem. Eng. Data* Vol. 60, PP. 2906-2914, 2015.
- [5]. B. Kvamme, T. Kuznetsova, B. Jensen, S. Stensholt, J. Bauman, S. Sjøblom, K.N. Lervik, "Consequences of CO₂ solubility for hydrate formation from carbon dioxide containing water and other impurities," *PCCP* Vol. 16, PP. 8623 – 8638, 2014.
- [6]. T. Maekawa, "Equilibrium conditions for gas hydrates of methane and ethane mixtures in pure water and sodium chloride solution," *GJ*, Vol. 35, PP. 59-66, 2001.
- [7]. G. D. Holder, J. H. Hand, "Multi-phase equilibria in hydrates from methane, ethane, propane and water," *AIChE J.*, Vol. 28, PP. 440-447, 1982.
- [8]. H.H. Reamer, F.T. Selleck, B. H. Sage, "Some Properties of Mixed Paraffinic & Other Olefinic Hydrate," *Trans. Am. Inst. Min., Metall. Pet. Eng.*, Vol. 195, PP. 197-202, 1952.
- [9]. G. Soave "Equilibrium constants from a modified Redlich-Kwong equation of state," *Chem. Eng. Sci.*, Vol. 27, PP. 1197-1203, 1971.
- [10]. B. Kvamme, T. Kuznetsova, P.-H. Kivelæ, "Adsorption of water and carbon dioxide on hematite and consequences for possible hydrate formation," *PCCP* Vol. 14, PP. 4410-4424, 2012.
- [11]. H.K. Ebbrell "The composition of Statoil (Norway) gas well Troll 31/6-6 [Internet]. [cited 2017-01-18]. Available from: http://www.npd.no/engelsk/cwi/pbl/wellbore_documents/127_05_31_6_6_6_The_Composition_of_Statoil_Gas_Well.pdf
- [12]. B. Kvamme, M. Qasim, K. Baig, P. H. Kivelæ, J. Bauman, "Phase field theory modeling of methane fluxes from exposed natural gas hydrate reservoirs," *International Journal of Greenhouse Gas Control.*, Vol. 29, PP. 263–278, 2014.
- [13]. K. Baig, B. Kvamme, T. Kuznetsova, J. Bauman, "The impact of water/hydrate film thickness on the kinetic rate of mixed hydrate formation during CO₂ injection into CH₄ hydrate," *AIChE journal.*, Vol. 61, Issue 11, PP. 3944–3957, November 2015.